Proceeding of the IEEE
International Conference on Robotics and Biomimetics
Dali, China, December 2019

Vision-Based Tactile Perception for Soft Robotic Hand *

Shixin Zhang◆ and Jianhua Shan

College of Mechanical Engineering
Anhui University of Technology
Maanshan, Anhui Province, China

zsx1723190077@163.com; 379751793@qq.com

Bin Fang◆*, Fuchun Sun* and Huaping Liu

Department of Computer Science and Technology
Tsinghua University
Beijing, China

fangbin@ tsinghua.edu.cn; hpliu@tsinghua.edu.cn;
fcsun@tsinghua.edu.cn

***Abstract* – The innovative vision-based tactile perception for soft robotic hand is proposed in this paper. The soft finger consists of a coloured elastic inner chamber, an outer structure, an endoscope camera, and a sealing device. The camera is used to capture the images of the inner chamber for tactile perception of soft robotic hand. Firstly the design and fabrication of the soft hand is descripted. Then the algorithm of recognizing the bending posture is proposed. The color regions boundary of image is extracted, and the convolutional neural networks is deduced to estimate the bending posture. The referred points from the boundary are selected, and the bending direction and the object surfaces' profile can be obtained by tracking displacement of the points. Finally, several experiments are designed and the results show the effectiveness of the proposed method and the superior performance of vision-based tactile perception.**

***Index Terms* - visual sensor; soft finger; tactile perception.**

I. INTRODUCTION

The hand plays an important role in human life. Its abundant perception capabilities can help human grasp objects effectively. A number of researches focus on the hand perception. [1] shows that the tactile corpuscle exists in deep skin, which contains sensitive nerve cells. When the nerve cell senses pressure, it sends a tiny electrical signal, which travels with the nerve fibers to the brain, and then human can feel the touch. When the finger touches the object's surface, the vibrations are sensed by activate receptors and the object's properties are perceived [2]. During the finger bending, the vibrations generate from joints activate receptors to make brain recognize the bending posture [3].

In order to make robotic hand intelligent like human, the researchers combined varieties of sensors based on physics or optics mechanism for perception. For the soft robotic hand, the sensors are required to be flexible and fit the structure of hand. The one of commonly used sensors is resistive sensor [4-6] that is made of specific material. According to recognize the value of resistance, the bending curvature can be indicated. Another common sensor is optical fiber sensor [7-8], which utilizes the principle of optical dissipation to measure the curvature. Besides, magnet and hall sensor [9] is also used. However, above sensors have the limitations that multiple bending directions or multi-modal tactile information are hard to measure.

The visual sensors have wide vision field and spatial resolution, which the captured images contain abundant feature information relating with perception. Based on the visual sensors, the researchers have obtained the distribution of force [10-12], slip and shear force [13-14], object texture [15-16] and other perception information [17]. The sensors consist of a CCD camera, acrylic plate and elastic body. When the elastic body where a metal coating is appended on the surface contact object, object texture can be showed by deformation of elastic body and light reflection. Whilst marker dots are added on the surface of elastic body, whose locations are changed when elastic body is forced. According to the displacements of dots, the sensors can recognize tactile and detect distribution of force including slip and shear force. Besides, there were also studies on perceiving edge of object [18-19]. However, the recent visual-based tactile sensor are mostly used for the fingertip.

In this paper, we propose a novel visual sensing mode used in soft finger. And the sensor is used in the four-finger soft hand. Without affecting structure and performance of soft finger, an inner chamber is fabricated in different color and a CCD camera is installed into root of finger, which is used to capture the images of color region of the inner chamber. When robotic hand grasps the object, the perception information including bending posture, bending direction and etc., can be obtained from the captured images. The remainder of this paper is organized as follows. Design and fabrication soft robotic finger is described in Section II. Section III introduces the proposed tactile perception algorithm. Section IV explains experimental scheme and results. Finally, conclusion and future work are described in Section V.

II. SOFT ROBOTIC FINGER DESIGN AND FABRICATION

In the four-finger soft hand, one finger is integrated with visual sensor, the others have no sensor. The vision-based soft finger consists of an outer structure, a color inner chamber, a sealing device, an endoscope camera and a pneumatic valve. The outer chamber has a certain hardness to support the soft finger. And the inner chamber is relatively soft. In the selection of color, it is required to be highly recognizable. In other words,

* This work is partially supported by National Natural Science Foundation of China with Grant No.91848206, Tsinghua University Initiative Scientific Research Program No. 2019Z08QCX15, Foshan-Tsinghua Innovation Special Fund (FTISF) No.2018THFS04 and National Natural Science Foundation of China with Grant No.U1613212.
◆denotes the same contributions ; *Corresponding author: fangbin@tsinghua.edu.cn, fcsun@tsinghua.edu.cn.

978-1-7281-6321-5/19//$31.00 ©2019 IEEE

there is a significant difference of RGB values between color regions. For example, red channel value is highest for red; blue channel value is highest for blue. Besides, the inner chamber require to be in close contact with the outer chamber. The sealing device is used to integrate the finger, camera and pneumatic valve. The camera embedded into the sealing device is used to capture the images of the deformation of the inner chamber. The camera is based on a pinhole model, whose resolution is 640×480 and the frame rate is as high as 30fps. The proposed soft finger with visual sensor is shown in Fig.1. Referring to human's finger, the length of soft finger is selected among 10 to 12 cm.

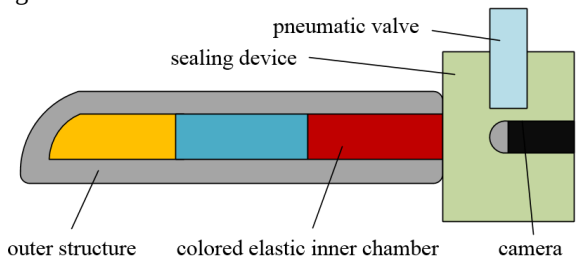

Fig.1 The structure of the proposed soft finger with visual sensor

A. *Design of the Chamber*

Based on imaging principle, the view of curve chamber is wider than linear chamber for the soft finger with visual sensor. As shown in Fig.2, the inner chamber is divided into three parts. Part a, b and c are respectively the projection lengths of three color arcs onto the centre line z. A, B, C and D are the endpoints of the three arcs. Segment DE is top of the inner chamber, which is perpendicular to the centre line. $\theta_{i,k}\,(i,k=\mathrm{B,C,D\ and}\, i\neq k)$ is the angle between the centre line and the connection of neighboring endpoints. According to the geometric relation, the locations of the four endpoints are orderly calculated.

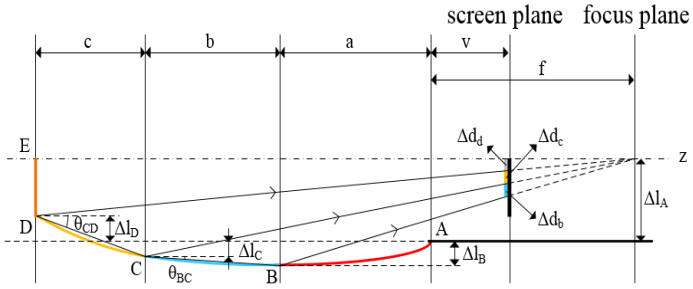

Fig.2 Principle analysis of imaging

$\Delta l_i\,(i=\mathrm{B,C,D})$ are the vertical distance between endpoints and center line. End-point A is coincident with end of the lens, where the distance $\Delta l_{\mathrm{A}}=4.1mm$. The relative location of endpoint B is as follows:

$$\frac{a+f}{f-v}=\frac{\Delta l_{\mathrm{A}}+\Delta l_B}{\Delta d_{\mathrm{b}}+\Delta d_{\mathrm{c}}+\Delta d_{\mathrm{d}}} \tag{1}$$

$$\Delta l_{\mathrm{C}}=\Delta l_{\mathrm{B}}-b*\tan(\theta_{\mathrm{BC}}) \tag{2}$$

where Δd_{b}、Δd_{c}、Δd_{d} are respectively the projection length of the segment DE, the yellow region and the blue region onto the screen plane. Referring to the parameters of the camera, image distance v=3.5mm and focal distance f=4mm.

Similarly, the relative location of endpoint C and D can be got. And there is a linear relation between the Δd_{b} and Δd_{c}.

$$\Delta d_{\mathrm{c}}=\eta*\Delta d_{\mathrm{b}} \tag{3}$$

where η is the imaging proportional coefficients of the yellow and blue region.

TABLE I. RELATION BETWEEN Δl_{D} 、 η AND θ_{CD}

$\Delta l_D(cm)$	$\theta_{CD}(°)$	η
0.759	15.888	1
0.633	13.640	0.9
0.507	11.348	0.8
0.381	9.019	0.7
0.255	6.659	0.6
0.129	4.277	0.5

The length of the inner chamber is a litter shorter than finger, which is selected as 10cm. Some parameters can be confirmed based on the finger size. Δl_{B} is chosen to be 2mm. The appropriate value of θ_{BC} ranges from 1° to 2°. In this case, each length of color region is respectively 4cm, 3cm, 3cm. Therefore only Δl_{D} , η and θ_{CD} become variables. Their relational table is established, as shown in Table I. Due to Δl_{D} locating among Δl_{A}, it satisfy both the imaging ratio and the size. Hence, η is recommended as 0.6. Above parameters are not constant, which can be adjusted according to design requirements.

B. *Design of Sealing Device*

Due to the adhesive power between the silicone and the sealing device is limited, soft finger is prone to rupture in inflating, which affects the gas impermeability and the performance of the soft finger. In order to solve this problem, the scheme is divided into two steps. Firstly, three teeth are designed in the sealing device. After sealing with the silicone, the teeth prevent the soft finger from getting out. Secondly, several holes are designed on the teeth to further enhance the resistance between the soft finger and the sealing device, when the holes are poured with liquid silicone for sealing and fixing. After silicone forming, it is locked by the teeth with the holes. The camera is embedded into the root of the sealing device to capture images of inner chamber. The pneumatic valve is embedded into the top of the device. The overall diagram of the sealing device is shown in the Fig.3. For the other soft finger, the pneumatic valve is installed in the root of device and camera hole is cancelled.

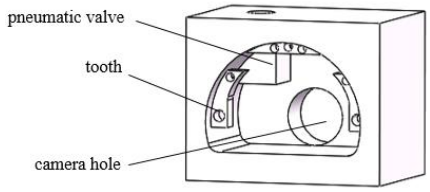

Fig.3 The diagram of sealing device used in soft finger with visual sensor

C. Fabrication

In the selection of materials, several factors should be considered: a certain amount of optical transparency, tensile strength, hardness, robustness and manufacturing complexity. There are two kinds of silicone for selection. Considering of easily coloring, the material uses colourless silicone A (SILGEL 612 A/B, Wacker Chemie AG, Germany) that its weight ratio is 1.7:1 and mixes with colored powder. To satisfy hardness, another uses silicone B (NASIL 4230A/B), whose weight ratio is 9:1. For the soft finger with visual sensor, its inner chamber is fabricated by silicone A and outer chamber is fabricated by silicone B. And the others are fabricated by silicone B.

The rigid molds are designed in Solidworks software and fabricated using PLA material by 3D printing. Its simplicity allows us to iteratively fabricate quickly. In Fig.4 (a)-(d), there are three molds, which respectively fabricate the inner chamber (mold A/B) and outer structure (mold C).

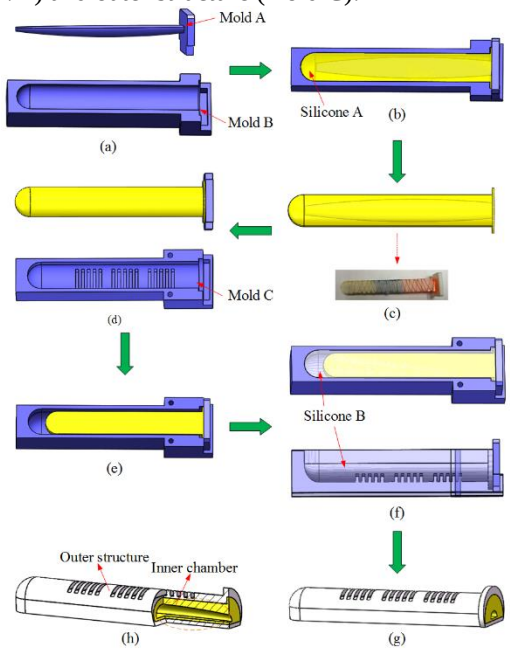

Fig.4 Schematic of the single soft finger fabrication process. (a) Mold A and B for inner chamber fabrication. (b) Pour silicone A/B into mold (the inner chamber color is three colors for soft finger with sensor, the others are not). (c) Limit the ductility of the inner chamber. (d) Mold C for outer structure fabrication. (e) Combine inner chamber with mold C. (f) Pour silicone B into mold. (g) The finished soft finger. (h) The overview of the soft finger with a cross section view which schematically illustrate the inner chamber and outer structure.

The multi-step molding process of soft finger is shown in Fig.4. Firstly, the uncured silicone A is poured into the mold A. The mold and uncured materials are then put in a vacuum oven for 30min for degassing and removing the air bubbles. And then it is heated to a temperature of 80°C for 2h in order to cure the material. This step requires to be repeated twice for fabricating three color inner chamber. Secondly, a piece of cloth is attached to the surface of inner chamber and is winded around by thin rope (see Fig.4(c)). Thirdly, the silicone B is poured into the mold B fixing with inner chamber. Then put it in a vacuum oven for 30min and heat for 1h. Finally, soft finger is inserted into sealing device and sealed with silicone B. The prototype of the proposed soft finger is shown in Fig.4 (h). For the other fingers fabrication, the process is the same except that the inner chamber is wholly fabricated by silicone B.

D. Assemble

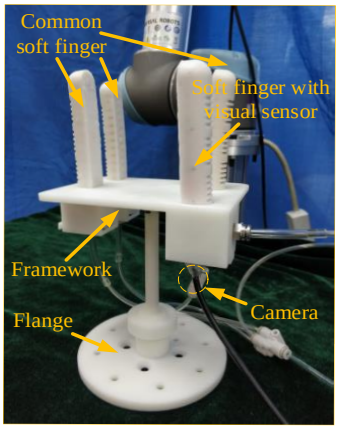

Fig.5 The design of four-finger soft hand. It consists of a soft finger with visual sensor, three common soft fingers, a framework and a flange. The flange is designed to connect with robot arm UR5.

The soft finger with visual sensor and three common fingers consist the four-finger soft hand as shown in Fig.5. In order to install into robot arm UR5, the flange is designed. In experimental section, the hand is used for grasping test to verify the performance of soft finger.

III. ALGORITHM

In this section, the recognition algorithm is divided into two parts. The method for recognizing the bending posture based on the convolutional neural network [20] is proposed. Then the algorithms of image processing and bending directions identification are deduced.

A. Algorithm of Recognizing the Bending Posture

a. Image Processing

There are two selections for input images. One is original image, another is processed image. For the original image, its shape and size of the boundary of color regions varies linearly as finger bending. It is the effective feature information. On the contrary, the values of RGB have huge difference in different light environment, which can generate noise to affect recognition effect. Therefore, original image is transformed into boundary image by image processing. Then boundary image is input into convolutional neural network.

The specific algorithm is as follows:

1) Image binarization. Based on Significant differences of colors in RGB values, the original image can be divided into different color regions by setting threshold value. Then the RGB values of neighboring regions are alternately set as one or zero.

2) Eliminate the noises. In order to get rid of the rest noises after step 1, dilatation corrosion operation is performed on the binary image with 3×3 core.

3) Edge detection. Using the edge detection function with OpenCV, the boundary of each region can be obtained. Record the locations of boundary, then renewed mark boundary in the resetting black image.

4) Image scaling. The size of image would affect complexity of network and the number of parameters. Therefore, scaling down the image can prevent these problems.

b. Network Structure

The processed boundary image only save effective feature, and the channel number of image reduces from three to one. It means simple convolutional neural network can satisfy recognition requirement. The convolutional layer is set four layers, which uses convolutional kernel to complete feature extraction from the upper layer to the next layer. The nonlinear activation layer completes the feature mapping from the upper layer to the next layer through the nonlinear function. The activation function is selected as ReLu [21] whose gradient is equal to 1 when value is more than 0. It is helpful to solve the convergence problem. Convolutional layer and activation layer are as a layer. The pooling layer is used to down sample, which benefit to reducing the dimension of the feature map and parameter numbers. Due to that input image is simplified, whose feature information could loss after pooling layer, the network don't adopt pooling layer. Finally, a fully connected layer is connected with the last convolutional layer. The whole structure is shown in Fig.6.

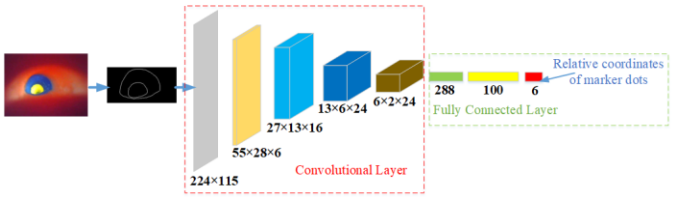

Fig.6 The structure of convolutional neural network

c. Optimization

The bending posture is presented by locations of four marker dots, where fourth marker dot is as reference dot. Therefore the results of network is returned output of relative coordinates of three marker dots by computed Mean Square Error(MSE). The network is optimized using an Adam [22], which we use a large learning rate (0.003). The initial regularization weight is set as 0.01. Considering of training difficulty of different marker dots, loss weight is adopted.

$$L_r = \beta_i \sum_{i=1}^{3} L_{ri} = \beta_i \sum_{i=1}^{3} \{(\dot{x}_i - \hat{x}_i)^2 + (\dot{y}_i - \hat{y}_i)^2\} \quad (4)$$

where L_r and L_{ri} is called Mean Square Error(MSE)[29] loss function. L_{ri} represents regression loss of each marker dot. $(\dot{x}_i, \dot{y}_i)$ is predicted relative coordinates, and $(\hat{x}_i, \hat{y}_i)$ is ground relative coordinates. And β_i is loss weight.

B. Algorithm of Tracking Location Change of Color Regions

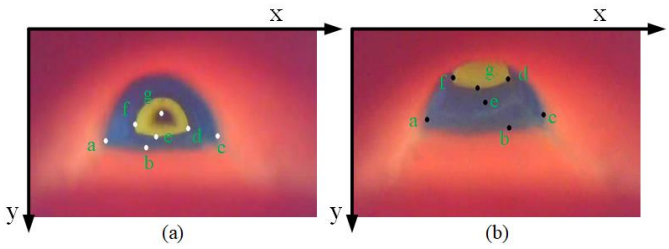

Fig.7 The reference points in initial state and bending state. a, b, c, g are leftmost, lowest, rightmost and center point of blue region respectively. d, e, f are leftmost, lowest, rightmost point of yellow region respectively. Each image has a coordinate system so that each pixel point has coordinate.

We classify bending direction as up down left and right. During bending process, it is found that the color regions move to bending direction. Therefore, bending direction can be recognized according to identify direction of color regions. Then some reference points are selected from boundary of color regions, whose movement can be tracked to indicate movement direction of color regions. Based on image processing, the reference points are available. In selection of reference marker points, there are seven kinds of points that can be attempted, which are lowest, leftmost, rightmost pixel point of the blue and yellow region and center point of blue region. These points can be easily made sure from each image, which means the points can be continuously tracked in Fig.7.

For these points, the movement of the lowest points of color regions and center points is most obvious in Y axis. In addition, the movement of the leftmost and rightmost points of color regions and center points is most remarkable in X axis. Therefore, they can be divided into two categories again. When bending to up and down, Y coordinates of lowest points of color regions and center points are tracked to recognize bending direction. When bending to left and right, X coordinates of the other points are used for recognition. The results of linear change of these points during bending are presented in the experimental section. Based on the results, select the suitable points.

The original image is processed to extract reference points. The coordinates can be obtained: x_i (X coordinates of reference points) and y_j (Y coordinates of reference marker points). Then, comparing to initial coordinates values, calculate the difference values of coordinates Δx_i and Δy_j. Find the maximum absolute value between Δx_i and Δy_j. Considering that little displacement of points could be confused with little errors of image recognition, a threshold value is set. If maximum absolute value is less than the threshold value, finger is considered as initial state. Else, when the maximum absolute value is from Δx_i and if $\Delta x_i > 0$, the direction is recognized as right; if $\Delta x_i < 0$, the direction is recognized as left. When the maximum absolute value is from Δy_j and if $\Delta y_j > 0$, the direction is recognized as down; $\Delta y_j < 0$, the direction is recognized as up. The specific algorithm is as following:

Algorithm 1 Identify bending directions

Data:

I (the total number of test samples)

X (x coordinate set including leftmost point, rightmost point and center point of blue boundary, $x_i \in X$)

Y (y coordinate set including lowest point and center point of blue boundary, $y_j \in Y$)

$\hat{X}$ (X in initial state)

$\hat{Y}$ (Y in initial state)

T (threshold value)

The initial state, up, down, left, right are present by number 0-4.

Input: X, Y

for t=1 to I **do**

$\Delta X = X - \hat{X}$

$\Delta Y = Y - \hat{Y}$

if Max(|($\Delta X \cdot \Delta Y$)|) < T

print 0

else

if Max $\in \Delta X$

Locate index of Max in ΔX as i.

if $X_i > 0$ **print** 4 **else** **print** 3

end if

else

Locate index of Max in ΔY as j.

if $y_i > 0$ **print** 2 **else** **print** 1

end if

end for

Besides, the magnitude of displacements can also reflect bending degree. The displacement is larger, the bending degree is larger; otherwise not. When finger slide to contact objects, the surface makes finger deform differently. According to track referred marker points, their displacements can be obtained and used to represent the features of object surface.

IV. EXPERIMENTS

A. The Test of Soft Finger Performance

The performance of soft finger by hand grasping objects in different postures are tested. For different objects, the soft finger can adapt their shape and size quickly as shown in Fig.8. The four fingers grasp objects tightly and make objects not fall down in horizontal or vertical state. The results show appending visual sensor don't affect grasping performance. Meanwhile the soft finger multi-perception is realized by visual sensor. In the Fig.8C, the finger can identify its bending direction; in the Fig.8D, the finger can detect feature of object surface; in the Fig.9, the finger can also recognize it's bending posture. In the following experiments, the above results will be demonstrated.

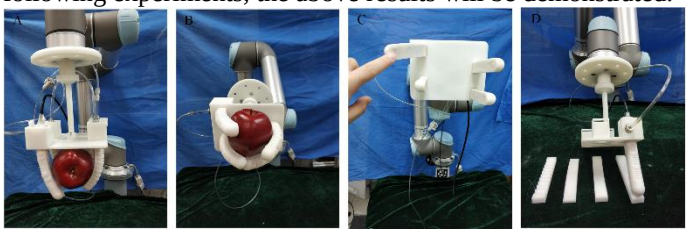

Fig.8 The capabilities of the hand. A. Grasp object in vertical. B. Grasp object in horizontal. C. Identify bending directions. D. Slide to touch object to recognize surface feature.

B. Recognition of Bending Posture

The outer camera (Intel RealSense SR300) is used to capture label images, where the locations of marker dots can be obtained. The outer and inner camera record a video at the same time. Each inner chamber image matches a label image. The inner chamber images are as sample set and locations of marker dots are as a label set.

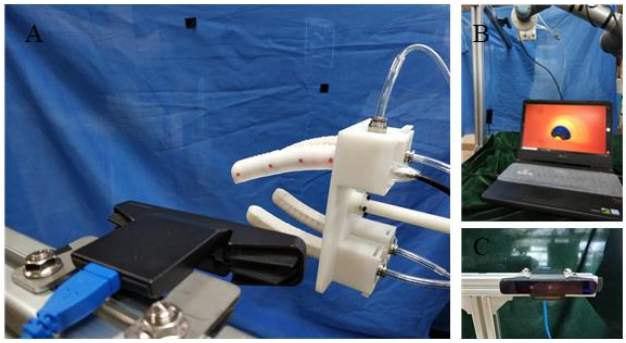

Fig.9 The collection of samples and labels. A. Use outer camera to capture label images. B. The inner camera is connected with computer by USB to capture the inner chamber images. C. The outer camera is selected as Intel RealSense SR300.

The result shows the errors and dispersion degree without appending loss weight in Fig.10(a) and Fig.11. The majority predicted dots keep away from the ground dots. Comparing with three category of dots, it is found that the recognition effect of third dot is acceptable. However, the result is worse as distance increases. In other words, the distances of dots determine the difficulty of optimization. Therefore, adjust the proportion of optimization by appending loss weight. The dot's errors and dispersion degree are more serious, the value of loss weight is larger; otherwise not.

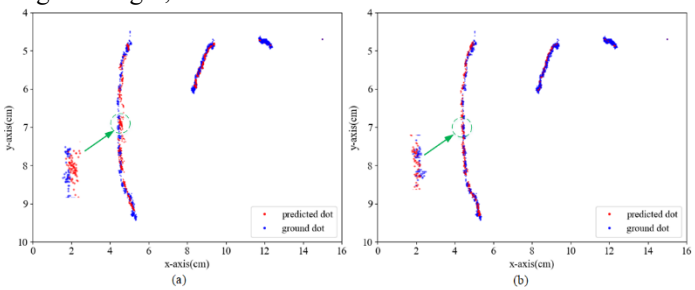

Fig.10 The distribution of predicted dots and ground dots

The result is computed with appending loss weight in Fig.10 (b) and Fig.11. It is observed that the errors and dispersion degree are improved obviously. In Fig.10 (b), the

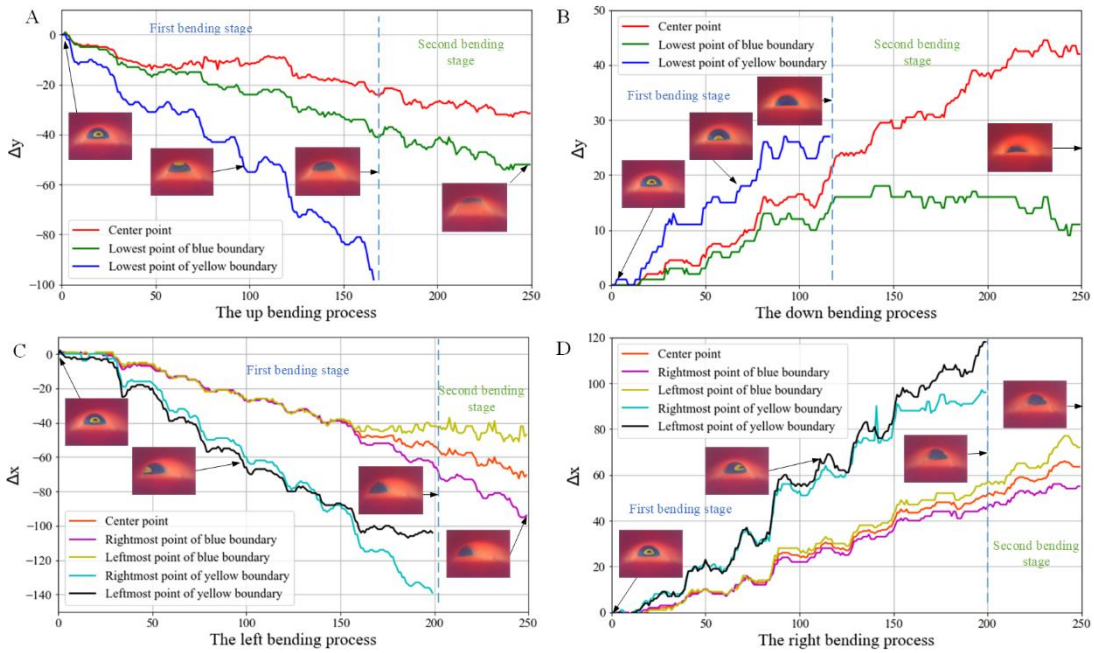

Fig.12 The linear relationship between reference dots and bending directions. A, B, C and D present linear relationship in up, down, left and right direction. The bending process is divided into two stage. One is that the size of yellow region is decreased. Another is that yellow region is disappeared and blue region is decreased continuously. For up and down direction, track displacement of y coordinates. For left and right direction, track displacement of y coordinates.

distribution of marker dots is much denser. And the predicted marker dots are close to the ground marker dots. In Fig.11, the errors and variance of marker dots are decreased, especially is the fourth marker dot. That means improvement of the fourth marker dot also promotes improvement of the others. In Fig.13, the inner chamber images also can reflect different objects' size.

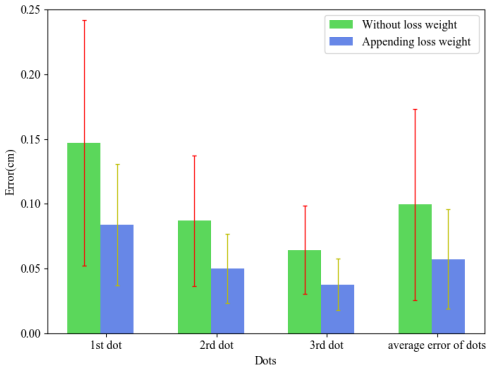

Fig.11 The error distribution of predicted dots without loss weight and appending loss weight

C. Identifying Bending Direction

The inner chamber images of four bending directions are captured. Each bending process is completed by manual. And the seven reference points are selected to represent image changing. As bending, the displacements of reference points are computed. The relationship between reference points and bending process can be obtained, as shown in Fig.12. In each bending direction, the process can be divided into two stages. One is that the size of yellow region is decreased. Another is that yellow region is disappeared and blue region is decreased continuously.

The curves have fluctuation mainly due to the shake during artificial bending process. Besides, a few errors of image recognition could also lead fluctuation. However, these interference can still be recognized, which means the image recognition precision is high. Not only that, it is found that all curves increase or decrease linearly, where the variation range of curves relating to blue region is instability. However, the variation of curves relating to yellow region is most obvious. It means these points is more sensitive than the others for recognizing a little change of image.

In order to assess the effect of recognition, we select 300 inner chamber images at random in each bending direction. The referred points of blue region are selected to track. The reference points of yellow region is not adopted that the yellow region cannot be captured all the time throughout the bending process. Based on the algorithm, the recognition of bending direction is realized. In Table II, the result shows that a few recognition faults without setting the threshold value. Because the slight displacement of wrong direction is maximum so that fault is occurred. If set a threshold value, the images in the slight change are identified as initial state. Therefore, the accuracy is increased.

D. Recognition of Object Surface Feature

The soft hand is installed in the robot arm UR5 as shown in Fig.8D. Control the arm so that the soft hand touches the object surface and bends slightly. The experimental objects are produced by 3D printer, whose surfaces are selected as flat surface, concave surface, convex surface and rough surface respectively. Then the robotic arm moves to make soft finger slid to touch the object. Based on tracking displacement of reference points, we reconstruct the profile of the surfaces in

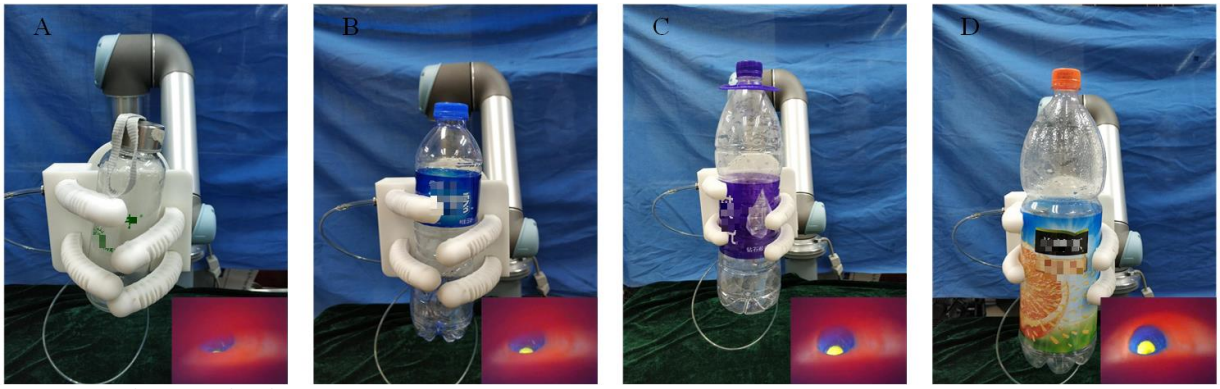

Fig.13 The recognition of object surface feature. A. A glass bottle, its diameter is 48mm. B. A common mineral water bottle, its diameter is 62mm. C. A medium mineral water bottle, its diameter is 82mm. D. A larger juice bottle, its diameter is 92mm. Different object size, the bending degree is different. According to recognize the inner chamber image, it is possible that the obtained bending posture estimates the object size and classify objects.

Fig.14. From these data, it is found that the image can clearly present feature of object surface. Although curve fluctuates slightly due to a few recognition errors, the results are not affected.

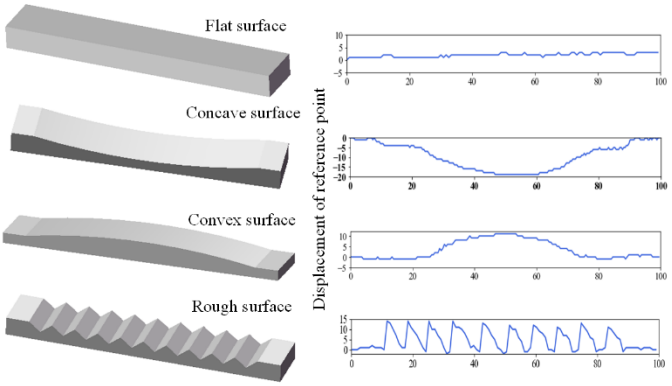

Fig.14 The profile is reconstructed by tracking displacement of reference points. Every displacement unit is a pixel, so that the fluctuation is like a ladder.

V. Conclusion and Future Work

In this work, we propose an innovative visual-based tactile perception for soft robotic hand. The visual sensor don't affect the performance of soft finger. Furthermore the finger can realize multi-perception. Based on convolutional neural network recognizing boundary of color regions, the relative coordinates of marker dots can be obtained, which are used to present bending posture of finger. Appending loss weight adjusts optimization difficulty, which make prediction precision improve further. According to track the displacement of referred points, the movement direction of color regions can be identified so that confirm bending direction. Based on the magnitude of displacement, the feature of object surfaces can be indicated.

Our experimental results demonstrate that visual mode can indeed simulate the perception mode of finger. However, we observe several points that can improve recognition effect. Firstly, the boundary region between color regions sometimes is not recognized effectively. Selecting a higher resolution camera can improve imaging quality to ease the problem. Secondly, the yellow region is more sensitive to deformation of soft hands. Therefore, its imaging scale can be increased. Finally, the more sample data can be captured, which can improve network's generalization. In future, more perception capabilities can be developed like identification of force and texture recognition.

Acknowledgment

This work was jointly supported by National Natural Science Foundation of China with Grant No.91848206, U1613212, Foshan-Tsinghua Innovation Special Fund

TABLE II The result of recognizing bending directions

Ground direction \ Predicted direction	Threshold value (Yes/No)	Initial state	Up	Down	Left	Right	Accuracy
Up	No	3	296	0	0	1	99.67%
	Yes	9	291	0	0	0	100%
Down	No	0	0	292	8	0	97.33%
	Yes	9	0	288	3	0	99%
Left	No	0	0	7	288	5	96%
	Yes	15	0	0	285	0	100%
Right	No	0	0	0	0	300	100%
	Yes	8	0	0	0	292	100%

No.2018THFS04 and Tsinghua University Initiative Scientific Research Program No.2019Z08QCX15.

REFERENCES

[1] Johansson, Roland S., and Åke B. Vallbo., "Tactile sensory coding in the glabrous skin of the human hand," Trends in neurosciences, vol. 6, pp. 27-32, 1983.

[2] Fagiani, Ramona, et al. "Tactile perception by friction induced vibrations," Tribology International, vol. 44, no. 10, pp. 1100-1110, 2011.

[3] Maeno, Takashi, Kazumi Kobayashi, and Nobutoshi Yamazaki., "Relationship between the structure of human finger tissue and the location of tactile receptors," JSME International Journal Series C Mechanical Systems, Machine Elements and Manufacturing, vol. 41, no. 1, pp. 94-100, 1998.

[4] Farrow N. and Correll N., "A soft pneumatic actuator that can sense grasp and touch," 2015 IEEE/RSJ International Conference on Intelligent Robots and Systems (IROS), pp. 2317-2323, 2015.

[5] Nassour J., Ghadiya V., Hugel V., and H. Hamker F., "Design of new Sensory Soft Hand: Combining air-pump actuation with superimposed curvature and pressure sensors," 2018 IEEE International Conference on Soft Robotics (RoboSoft), pp. 164-169, 2018.

[6] Elgeneidy K., Neumann G., Pearson S., Jackson M., and Lohse N., "Contact Detection and Size Estimation Using a Modular Soft Gripper with Embedded Flex Sensors," 2018 IEEE/RSJ International Conference on Intelligent Robots and Systems (IROS), pp. 498-503, 2018.

[7] Huichan Zhao, Kevin O Brien, Shuo Li, and Robert F. Shepherd, "Optoelectronically innervated soft prosthetic hand via stretchable optical waveguides," Science Robotics, vol. 1, no. 1, pp. 7529, 2016.

[8] Xu R., Yurkewich A., and V. Patel R., "Curvature, Torsion, and Force Sensing in Continuum Robots Using Helically Wrapped FBG Sensors," IEEE Robotics and Automation Letters, vol. 1, no. 2, pp. 1052-1059, 2016.

[9] Ozel S., H. Skorina E., Luo M., Tao W., Chen F., Pan Yixiao, and D. Onal C., "A composite soft bending actuation module with integrated curvature sensing," 2016 IEEE International Conference on Robotics and Automation (ICRA), pp. 4963-4968, 2016.

[10] Fang B., Sun F., Yang C., Xue H., Chen W., Zhang C., Guo D., and Liu H., "A Dual-Modal Vision-Based Tactile Sensor for Robotic Hand Grasping," 2018 IEEE International Conference on Robotics and Automation (ICRA), pp. 1-9, 2018.

[11] Aquilina K., A. W. Barton D., and F. Lepora N., "Principal Components of Touch," 2018 IEEE International Conference on Robotics and Automation (ICRA), pp. 1-8, 2018.

[12] Donlon E., Dong S., Liu M., Li J., Adelson E., and Rodriguez A., "GelSlim: A High-Resolution, Compact, Robust, and Calibrated Tactile-sensing Finger," 2018 IEEE/RSJ International Conference on Intelligent Robots and Systems (IROS), pp. 1927-1934, 2018.

[13] Li J., Dong S., and Adelson E., "Slip Detection with Combined Tactile and Visual Information," 2018 IEEE International Conference on Robotics and Automation (ICRA), pp. 7772-7777, 2018.

[14] W. McInroe B., L. Chen C., Y. Goldberg K., Y. Goldberg K., Bajcsy R., and S. Fearing R., "Towards a Soft Fingertip with Integrated Sensing and Actuation," 2018 IEEE/RSJ International Conference on Intelligent Robots and Systems (IROS), pp. 6437-6444, 2018.

[15] Yuan W., Mo Y., Wang S., and H. Adelson E., "Active Clothing Material Perception Using Tactile Sensing and Deep Learning," 2018 IEEE International Conference on Robotics and Automation (ICRA), pp. 1-8, 2018.

[16] Luo S., Yuan W., Adelson E., G. Cohn A., and Fuentes R., "ViTac: Feature Sharing Between Vision and Tactile Sensing for Cloth Texture Recognition," 2018 IEEE International Conference on Robotics and Automation (ICRA), pp. 2722-2727, 2018.

[17] Yuan, Wenzhen, et al., "Shape-independent hardness estimation using deep learning and a gelsight tactile sensor." 2017 IEEE International Conference on Robotics and Automation (ICRA), pp. 951-958, 2017.

[18] Pestell N., Lloyd J., Rossiter J., and F. Lepora N., "Dual-Modal Tactile Perception and Exploration," IEEE Robotics and Automation Letters, vol. 3, no. 2, pp. 1033-1040, 2018.

[19] Ward-Cherrier., Benjamin., et al. "The tactip family: Soft optical tactile sensors with 3d-printed biomimetic morphologies," Soft robotics,vol. 5, no. 2, pp. 216-227, 2018.

[20] Krizhevsky, A., Sutskever, I., and Hinton GE. "Imagenet classification with deep convolutional neural networks," Advances in neural information processing systems, pp. 1097-1105, 2012.

[21] Agarap, A. F. "Deep learning using rectified linear units (relu)," arXiv preprint arXiv, vol. 1803, no. 08375, 2018.

[22] Kingma, Diederik P., and Jimmy Ba. "Adam: A method for stochastic optimization," arXiv preprint arXiv, vol. 1412, no. 6980, 2014.